P-wave Velocity Structure of the Lower Crust and Uppermost Mantle Beneath the Sichuan-Yunnan (China) Region

Zhi Wei[1,2] and Li Zhao[1,2*]

1. *School of Earth and Space Sciences, Peking University, Beijing, 100871, China*
2. *Hongshan National Geophysical Observatory, Beijing, 100871, China*

Highlights

1. We obtain a high-resolution P-wave tomography model for the lower crust and uppermost mantle of the Sichuan-Yunnan region.
2. Our model indicates a coupling between the surface deformation and the material flow in the lower crust.
3. The crust-mantle transition zone in the eastern margin of Songpan-Ganzi Block may also be influenced by weak materials from deep mantle.

* Correspondence to: `lizhaopku@pku.edu.cn`

Abstract

We conduct a tomographic inversion for the 3-D P-wave velocity structure in the lower crust and uppermost mantle of the Sichuan-Yunnan region in the southeastern margin of the Tibetan Plateau. A total of 43,450 reliable arrival times of P waves are picked from over 300,000 regional seismic records using an automatic algorithm based on deep learning. A two-stage iterative inversion process is adopted in which events are relocated in the process, leading to a significant reduction in traveltime residuals. A statistical resolution matrix analysis suggests that our model has an optimal spatial resolution length of ~0.4° in the lower crust and ~0.2° in the uppermost mantle. Our 3-D model shows that both the lower crust and uppermost mantle in the region are characterized by strong lateral heterogeneities. The unusually low velocities in the lower crust may indicate the existence of lower crustal flow, whereas the high velocity anomalies in the uppermost mantle in and around the Sichuan-Yunnan Rhombic Block may be an important factor in preventing the ductile materials in the lower crust moving eastward. Our model also indicates a coupling between the surface deformation and the material flow in the lower crust. Finally, the lower crustal flow may influence the materials immediately below the Moho interface beneath the Sichuan-Yunnan Rhombic Block, and the crust-mantle transition zone in the eastern margin of Songpan-Ganzi Block may be influenced by both the lower crustal flow and the upwelling warm materials from below.

Key words: Sichuan-Yunnan region; lower crust; uppermost mantle; P-wave velocity structure; lower crustal flow

1. Introduction

The Sichuan-Yunnan region located in the southwestern margin of the Tibetan Plateau has been under continuing crustal deformation since the collision between the Indian and Eurasian plates ~65 Ma ago. As an extremely complex transition zone between the uplifted Tibetan Plateau in the west and the relatively stable Yangtze craton in the east, a series of large-scale active fault zones have formed in the region (Figure 1), including the Longmenshan Fault Zone (LMSFZ), Xiaojiang Fault Zone (XJFZ), Lancangjiang Fault Zone (LCJFZ), Luzhijiang Fault Zone (LZJFZ), Lijiang-Xiaojinhe Fault Zone (LJ-XJHFZ), Jinshajiang Fault Zone (JSJFZ), and Red River Fault Zone (RRFZ). Most of the large earthquakes in the Sichuan-Yunnan region occur in and around these fault zones. Furthermore, these fault zones act as boundaries between the main tectonic blocks of this region. As a result, the region as a whole is under large-scale shear deformation, resulting in complex patterns of block motions involving translation, rotation and extrusion. For example, the Sichuan-Yunnan Rhombic Block (Figure 1) is moving in south-southeast direction with clockwise rotation and extrusion (Xu et al., 2003). The tectonic environment in this region is thus complex and requires continuous efforts to gather information from various disciplines, including and in particular seismology, to resolve the three-dimensional (3-D) structures at depth in order to understand the evolution and interaction of different tectonic blocks.

Previous studies have shown that the crust and upper mantle in the Sichuan-Yunnan region are generally characterized by specific influences that can be attributed to the Indian and Eurasian plate collision, such as the wide-spread low-velocity (e.g., Kan et al., 1986; Wang et al., 2003; Wang et al., 2016) and high-attenuation zones (e.g., Wei and Zhao, 2019; Zhao et al., 2013), large variation of crustal thickness (Wang et al., 2010), and the existence of a layer of high heat flow and high conductivity (Bai et al., 2010). Large-scale surface deformation with an obvious clockwise rotation can be seen in GPS observations in this region (e.g., Wang et al., 2001; Zhang et al., 2004; Wang and Sheng, 2020; Wang et al., 2021). However, various aspects of the movement of the deep crust and uppermost mantle, including the depth extent of the surface deformation, the existence and pattern of the lower crustal flow, and the nature of the interaction between the lower crust and uppermost mantle, still remain to be resolved.

With the increased deployment of digital broadband seismometers at the turn of the century, the Sichuan-Yunnan region has been the focus of a number of seismic studies (e.g., Zhang and Wang, 2009; Yao et al., 2010; Lu et al., 2013; Zhao et al., 2013; Chen et al., 2014; Liu et al., 2014; Bao et al., 2015; Legendre et al., 2015; Wei and Zhao, 2019). Based on the lithospheric P-wave velocity structure obtained from wide-angle seismic profiles, Zhang and Wang (2009) suggested that the surface deformation in Yunnan is decoupled from the lower crust flow, which is consistent with Royden et al. (1997) which, via geodynamic simulation, indicated that the lower crust in this region is weak enough to allow the upper crustal deformation to be decoupled from the materials below. Lu et al. (2013) found distinct velocity differences between the southern and

northern parts of the uppermost mantle in the Sichuan-Yunnan region from 2.5-dimensional inversions of the P- and S-wave velocity structures. Chen et al. (2016) reported a weak lower crust which allows for material flow there and revealed a complex crust-mantle coupling mechanism in the Yunnan region based on a 3-D azimuthally anisotropic S-wave velocity model constructed from teleseismic surface waves. Using ambient noise as well as teleseismic body and surface waves, Yang et al. (2020) obtained a crustal S-wave velocity model with a best horizontal resolution of 0.5°. They found widespread low-velocity zones in the mid-lower crust in the Sichuan-Yunnan region, and that the boundaries of the low-velocity zones correlate well with major fault systems. The seismic velocity models of the crust and uppermost mantle obtained in different studies are generally in good agreement in large-scale features, such as the high-velocity anomaly beneath the stable Sichuan Basin. However, models with higher resolution are necessary to confirm the existence of material flow in the lower crust, and to understand the interactions between the lower crust and uppermost mantle, which is still not well resolved by the existing seismic experiments in the region.

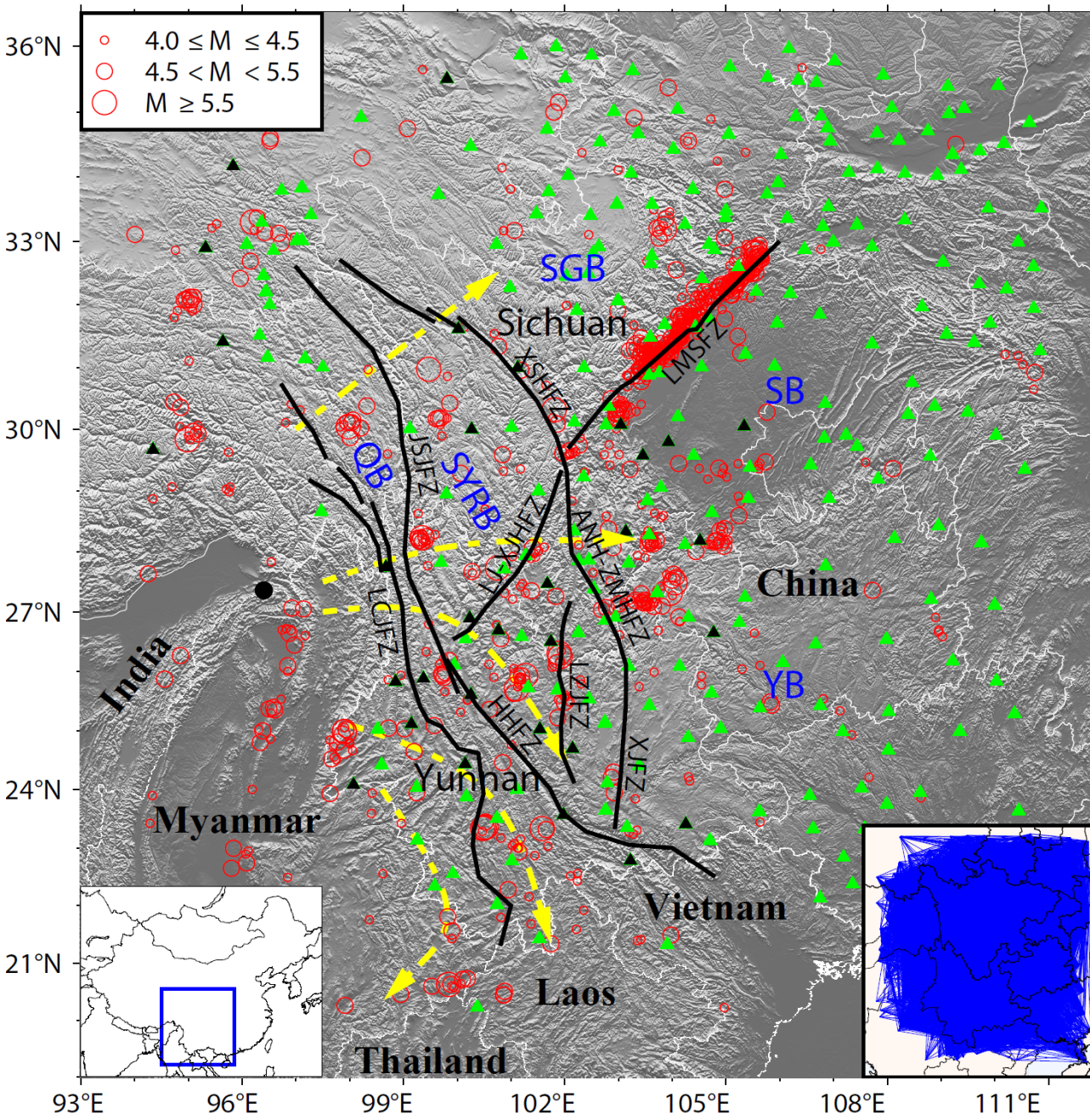

Figure 1 Map of tectonic environment of the Sichuan-Yunnan and surrounding regions with seismic stations, events and faults superimposed. Red circles and green triangles show respectively event and station locations selected for the P-wave velocity model inversion in this study. The black dot and triangles show

the locations of the event and stations whose records are displayed in Figure 2. Major active fault zones are shown by thick black lines with abbreviated names in black, including LMSFZ (Longmenshan Fault Zone), XSHFZ (Xianshuihe Fault Zone), ANH-ZMHFZ (Anninghe-Zemuhe Fault Zone), XJFZ (Xiaojiang Fault Zone), LJ-XJHFZ (Lijiang-Xiaojinhe Fault Zone), JSJFZ (Jinshajiang Fault Zone), RRFZ (Red River Fault Zone), LZJFZ (Luzhijiang Fault Zone), and LCJFZ (Lancangjiang Fault Zone). Major tectonic blocks are indicated by abbreviated names in blue, including SYRB (Sichuan-Yunnan Rhombic Block), SB (Sichuan Basin), SGB (Songpan-Ganzi Block), QB (Qiangtang Block), and YB (Yangtze Block). The yellow dashed lines with arrows show the general directions of the velocity field of crustal deformation (Wang and Shen, 2020). The plot in the lower-right corner shows the P-wave ray paths (43,540) coverage used in this study.

The strong crustal deformation and relative motions between various blocks make the Sichuan-Yunnan region one of the most tectonically active zones with a high level of earthquake activities. Frequently occurring small and moderate earthquakes, coupled with the deployment of increasing number of broadband seismic stations in recent years provide valuable data for us to improve the quality of regional structural images. In this study, we develop a high-resolution P-wave velocity model for the lower crust and uppermost mantle for the Sichuan-Yunnan region by applying the fast marching Method (FMM) of Rawlinson and Urvoy (2006) to a large dataset of P waves obtained by an automatic picking algorithm based on deep learning (Wang et al., 2019). The true resolution of the model has been estimated by the statistical resolution matrix approach (An, 2012). Our results provide further support for the existence of the lower crust flow and reveal more details on the complex structure of the uppermost mantle of the Sichuan-Yunnan region.

2. Data and Method

2.1 Seismic records

In this study, we use P waves recorded at regional distances. To ensure sufficient signal-to-noise ratio (SNR) for reliable P-wave onset time picking while avoiding the influence of source complexity, we choose events of magnitudes 4.0-6.2. This results in a total of 822 events selected in the Sichuan-Yunnan region from 1994 to 2020. Figure 1 shows the distributions of the events as well as the 284 stations used in this study. The events are mainly distributed in and around the major fault zones in the western part of the study region as expected, especially along the Longmenshan Fault Zone where the M_W7.9 Wenchuan earthquake occurred in 2008. On the other hand, most of the stations are located in the eastern part of the study region. In the end, we use a collection of more than 300,000 vertical-component broadband records downloaded from the data management centers of the China National Seismic Network (SEISDMC, doi:10.11998/SeisDmc/SN) and the Incorporated Research Institutions for Seismology (IRIS, http://www.iris.edu).

2.2 P-wave onset time picking and ray path coverage

In this study, we use the onset times of first arriving P waves in the epicentral distance range of 2.5°-15° to develop the regional P-wave velocity model. As show in the vertical projections of the ray paths in Figure 2, the first-arriving P waves in this distance range include the crustal Pg waves at shorter distances and Pn and upper-mantle diving P waves at larger distance.

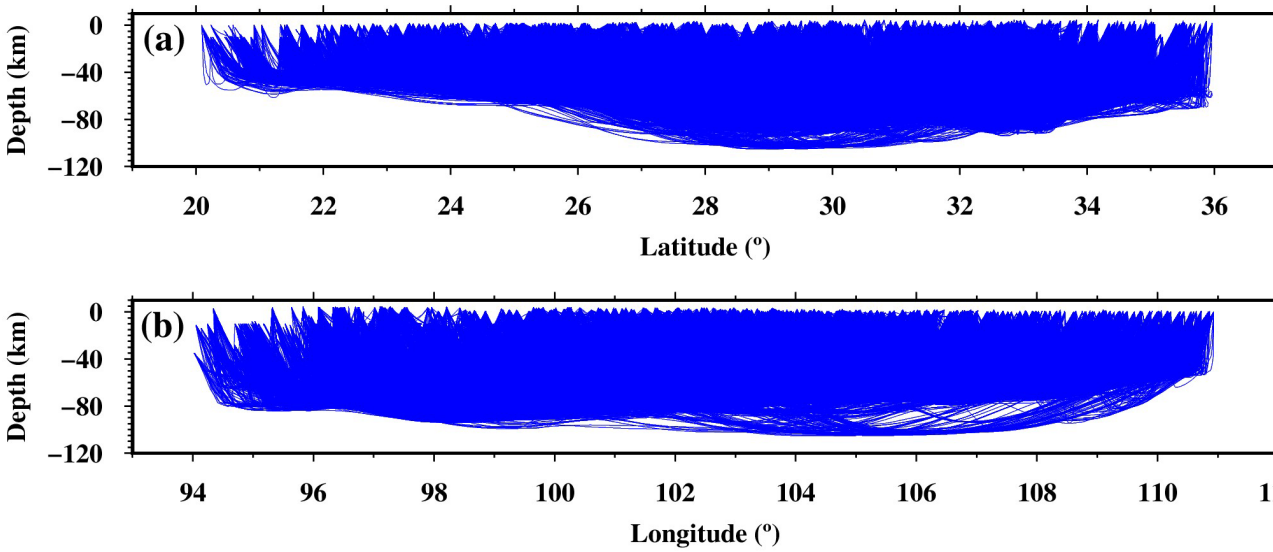

Figure 2 Projections of all ray paths used in this study onto vertical planes showing the depth distribution of the ray paths. (a) Projection onto the north-south plane. (b) Projection onto the east-west plane.

Picking the first-arrival onset times from more than 300,000 seismic waveforms manually is a tedious task, which is both inefficient and prone to human error. Effective algorithms have been developed in recent years based on machine learning to pick the arrival times of seismic phases from a large quantity of seismic records (e.g., Ross et al., 2018; Zhu and Beroza, 2019). In this study, we use the deep learning model PickNet of Wang et al. (2019) for our first-arrival onset time picking purpose. The PickNet model has been trained with ~500,000 manually checked first-arrival times and its validity has been tested for various datasets.

For each record, we cut a 20-s-long P-wave window centered at the theoretical first-arrival time in the AK135 velocity model (Kennett et al., 1995). The windowed waveforms are processed to have zero mean and normalized by maximum values before they are fed to the PickNet algorithm. An example is shown in Figure 3 for the 10 February 2019 M_W5.0 earthquake in the border region between Myanmar and India. Although all seismograms are processed by PickNet for automatic picking, we still visually checked all the picks to ensure their reliability. Some of the onsets in waveforms with lower SNRs tend to be unclear,

but PickNet still yields the picks. Those picks are removed from further analysis, and we end up with a total of 43,540 reliable first-arrival time picks for the subsequent P-wave tomography inversion.

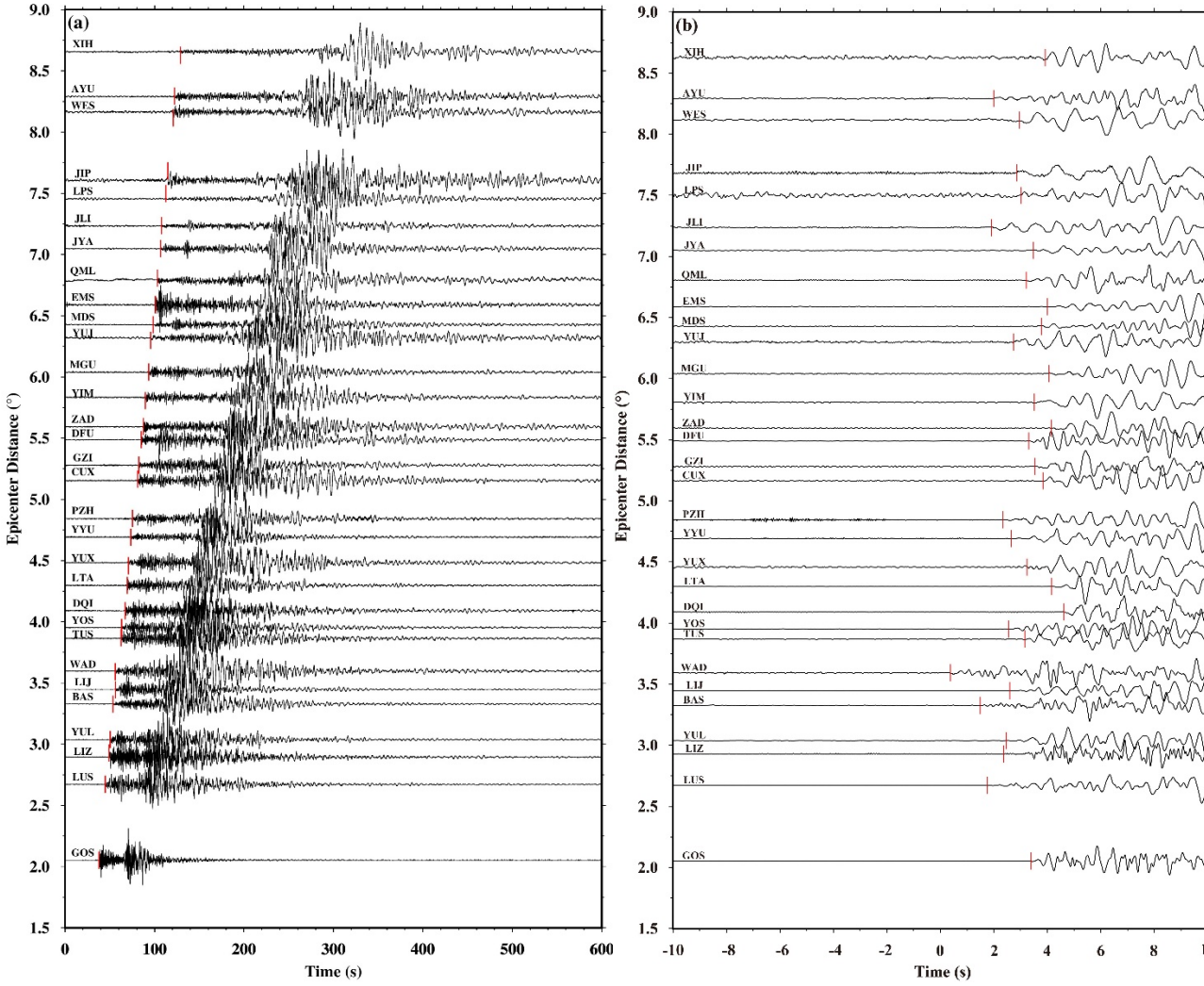

Figure 3 An example of the P-wave onset time picking by PickNet (Wang et al., 2019) using vertical-component records of the 10 February 2019 M_W5.0 event in the border region between Myanmar and India (epicentre and station locations shown by the black dot and triangles in Figure 1). The station name is given in the beginning of each trace, and the red vertical line shows the picked P-wave onset time. (a) 600-s long records starting from the earthquake original time. (b) Zoom-in views of the records in (a) in 20-s-long windows starting from 10 s before the theoretical P-wave arrival times in AK135 model (Kennett et al., 1995). All waveforms are self-normalized by the maximum amplitudes.

To evaluate the coverage of our dataset, we calculate the number of the first-arriving P-wave ray paths through each 0.2° × 0.2° cell at different depths, and the results are displayed in Figure 4. The ray path density distribution shows that both the lower crust and uppermost mantle (depth range 45-70 km) are generally well sampled by the dataset, with large parts of the region having ray paths of more than 150 in each cell. The density of the ray paths increases from the lower crust to the uppermost mantle. With the decrease of the takeoff angles for longer distances, sampling points at greater depths increase, particularly in the uppermost mantle where the ray paths are nearly horizontal, as shown in Figure 2. This implies that our dataset may provide better resolution in the uppermost mantle than that in the lower crust.

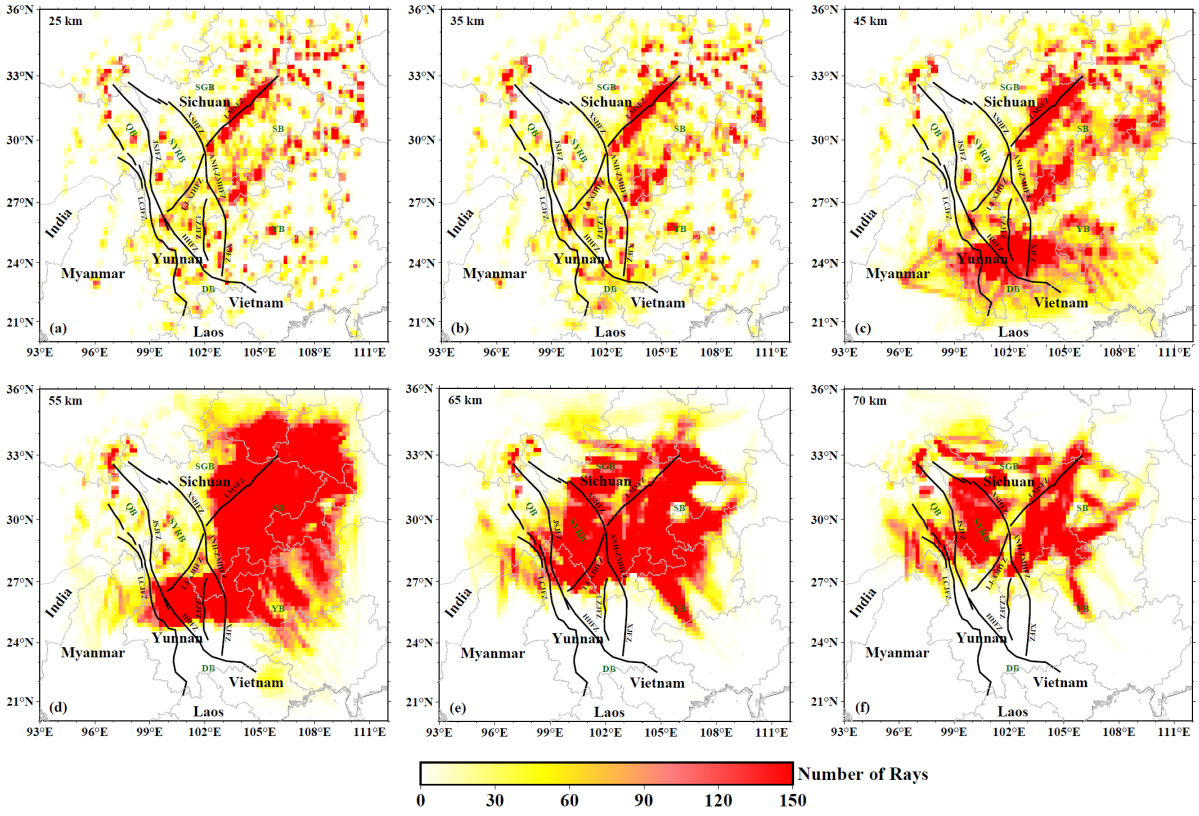

Figure 4 Number of ray paths within each 0.2° × 0.2° cell at several depths in the range of 25–70 km. Map features are the same as in Figure 1.

Although we have collected seismic records for event-station pairs with separations up to 15°, over 90% of the picked onset times come from Pg and Pn waves with epicentral distances smaller than 10°. This can be seen in the time-distance plot of all the data obtained in this study in Figure 5. The relatively high seismic attenuation of the Sichuan-Yunnan region (Wei and Zhao, 2019)

may have prevented the P waves turning in the uppermost mantle from propagating efficiently over longer distances. The limited number of data at shorter epicentral distances suggest that regions above the lower crustal may not be very well sampled, whereas the vertical profiles of the ray paths in Figure 2 show that structures deeper than 70 km are poorly constrained by our dataset. Based on the data and ray path distributions shown in Figures 2, 4 and 5, we focus our attention on the lower crust of the Sichuan-Yunnan region as well as the topmost part of the upper mantle in Sichuan and northern Yunnan.

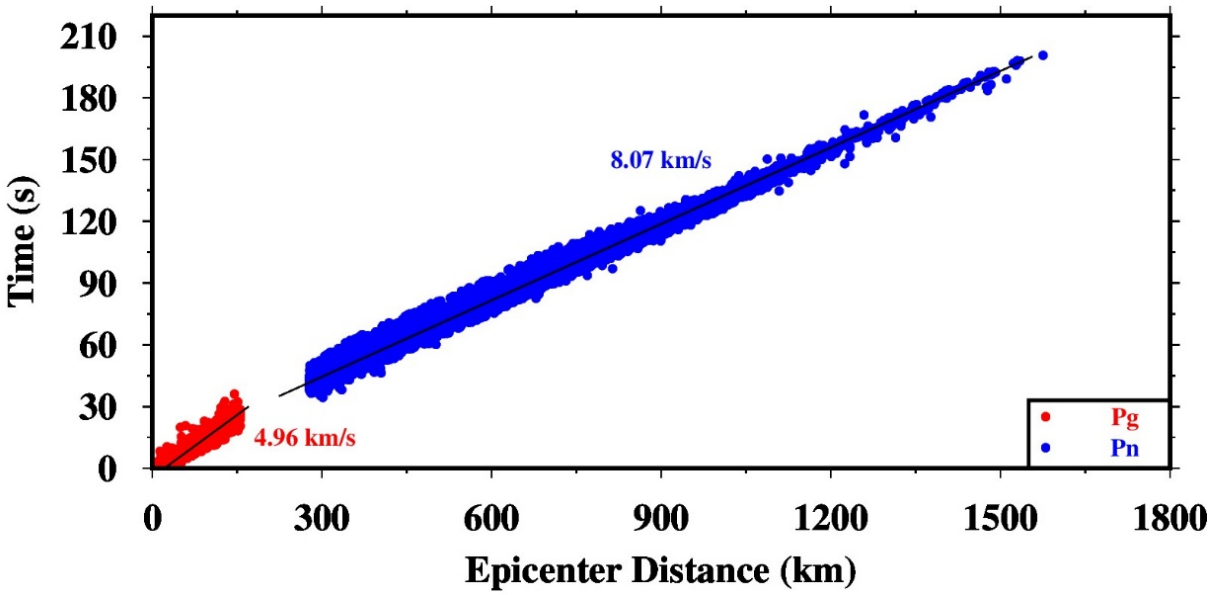

Figure 5 Time vs. distance plot of the onset times obtained by PickNet. Red dots are for Pg and blue ones are for Pn and P waves turning in the uppermost mantle. The black lines denote the apparent velocities of 4.96 km/s for Pg and 8.07 km/s for Pn.

2.3 Event relocation

The accuracy and reliability of seismic tomography are also dependent on the quality of the location results of the earthquakes, which may contain significant uncertainties since they are often obtained from routine event determinations based on 1-D Earth models. To minimize the biases in our tomography introduced by event location errors, we adopt an iterative inversion process during which the 3-D P-wave velocity model obtained from our inversion is used to relocate all of the contributing events. The relocation uses P-wave travel times calculated in the 3-D model by the multi-stage fast marching method (de Kool et al., 2006) and the neighbourhood algorithm (Sambridge and Kennett, 2001) in a global search for the hypocenters.

2.4 Tomography inversion

An optimal initial velocity model is often necessary for the success of tomographic inversions. In this study, we invoke the global 3-D lithospheric model LITHO1.0 (Pasyanos et al., 2014) as the starting model. Our tomography region spans the area from 20°N to 30°N in latitude, 93°E to 111°E in longitude, and from the surface down to 155 km in depth. We parameterize our model by a 3-D grid with grid spacing of 0.1° horizontally and 2.5 km vertically, which enables us to capture small-scale anomalies in regions where the ray paths are dense.

In this study, we adopt the inversion scheme FMM of Rawlinson and Urvoy (2006) which uses the multi-stage fast marching algorithm (de Kool et al., 2006) to compute the P-wave travel times in 3-D models and the subspace technique (Rawlinson et al., 2006) to iteratively solve the inverse problem of finding the model parameters that minimize the residual between the observed and model-predicted travel times with appropriate regularization parameters. We have conducted extensive inversion tests to find the optimal regularization parameters, and the final values of 0.1 and 5.0 are determined for the damping and smoothing constraints, respectively, leading to results with sufficient small-scale structural features but without unwarranted strong localized anomalies and sharp contrasts in velocities.

2.5 Resolution test

Checkerboard tests have often been used in seismic tomography studies to demonstrate how well an inversion can recover a model with a fixed pattern of heterogeneity distribution. A comprehensive assessment of the resolution of an inversion, however, requires the knowledge of the resolution matrix (e.g., Backus & Gilbert, 1968; Ritsemaetal et al., 2004), which has been used in the analyses spatial resolutions in tomography studies (e.g., Thurber, 1983; Barmin et al, 2001; Soldati and Boschi, 2005). However, in most inversion practices the exact resolution matrices require prohibitive amount of efforts to compute numerically, and various techniques have been developed to probe the properties of the resolution matrices without actually computing them. Here, we use the statistical resolution matrix approach of An (2012) to examine the spatial resolving power of our inversion. By inverting the synthetic data from a limited number of random models and comparing the input and recovered model pairs, we can probe the resolution matrix and determine the distribution of spatial resolution lengths of the tomography inversion. In this study, we use a total of 1200 random models, each of which is generated by adding random perturbations with maximum amplitude of ±7% to the initial model, to determine the horizontal spatial resolution lengths at different depths. The results are shown in Figure 6. Although still involving a large amount of computational labor, this is a practical and effective approach to evaluating the resolving power of the dataset in the inversion.

Figure 6 shows clearly that the resolutions are quite good for most part of the Sichuan-Yunnan region at all depths between 25 and 70 km with resolutions of ~0.4° in some regions in the lower crust and ~0.2° in most parts of the uppermost

mantle, consistent with our earlier assessment from the ray path distributions seen in Figures 2 and 4. In the lower crust, the region around the Longmenshan Fault Zone and most part of northern Yunnan are dominated by a resolution length of over 0.5°. The uppermost mantle under the Sichuan Basin, Yangtze Block and eastern part of the Songpan-Ganzi Block are mainly characterized by a resolution length of ~0.2°. With regard to the Sichuan-Yunnan Rhombic Block (SYRB), the resolution to the velocity in the uppermost mantle changes clearly with depth. For example, the small region southeast of the Lijiang-Xiaojinhe Fault Zone has excellent resolution at 55-km depth, while there is a large area northwest of the fault zone having excellent resolution at 70-km depth.

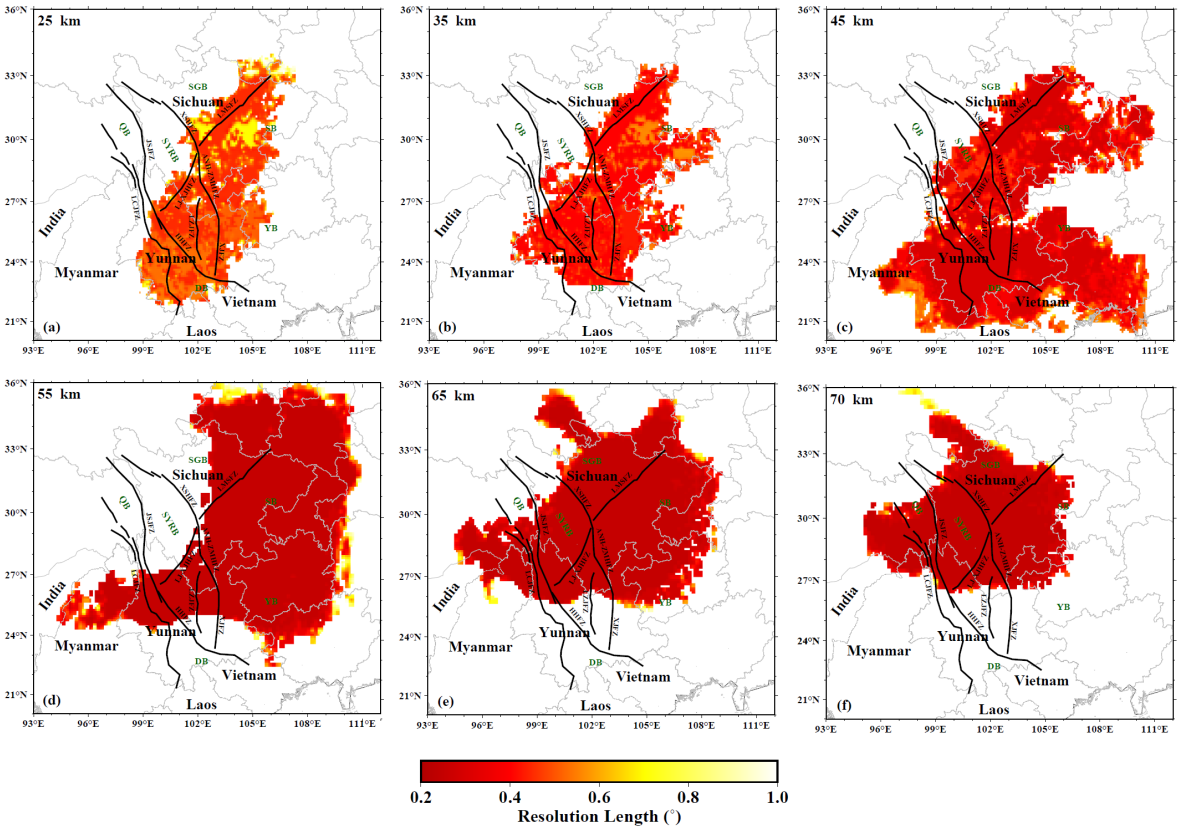

Figure 6 Spatial distributions of horizontal resolution lengths (in degrees) for several depths in the range of 25–70 km. Map features are the same as in Figure 4.

3. Result

Our final dataset contains 43,540 Pg and Pn onset times from 822 events to 284 stations. We use the FMM to invert this dataset in a two-stage iterative process for the P-wave velocity structure in the lower crust and uppermost mantle of the

Sichuan-Yunnan region. The first stage involves 6 inversion iterations starting from the initial LITHO1.0 model. The decrease of the root-mean-square (RMS) traveltime residuals with iteration number is shown in Figure 7(a). The total RMS residual decreases rapidly in the first few inversions but gradually levels off. Therefore, at the end of the first stage after the 6th inversion, we carry out a relocation of all events in the current model. Then, the inversion continues to the second stage until the RMS residual levels off again, and we choose to stop after the 10th iteration. Figures 7(b) and (c) show respectively the histograms of the residuals before and after the two-stage inversion. The residuals are distributed much more narrowly around zero after the inversion, testifying to the effectiveness of the tomography approach.

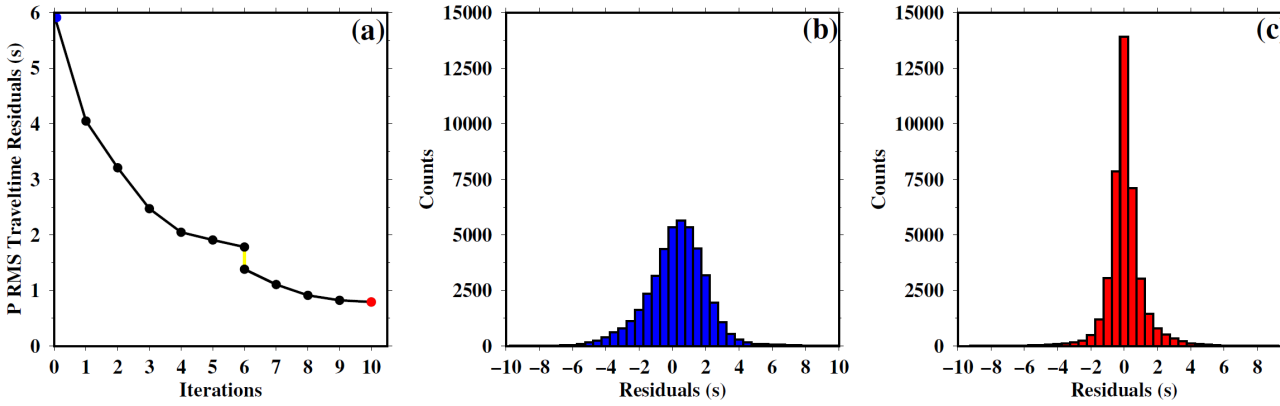

Figure 7 Decrease in the traveltime residuals during the two-stage iterative inversion. (a) Decrease in RMS traveltime residual with the iteration number. Events are relocated after the 6th iteration, hence the drop in the RMS traveltime residual. The iteration is terminated after the 10^{th} inversion. (b) Histogram of the traveltime residuals before the two-stage inversion. (c) Histogram of the traveltime residuals after the 10th iteration.

The P-wave velocity model obtained after the 10-iteration two-stage inversion is displayed in map views in Figure 8 for the lower crustal depths and in Figure 9 for uppermost mantle depths. Different color bars are used for different depth ranges to accommodate the difference in velocity values. Based on the resolution length estimation shown in Figure 6, we only present the portions of the model where the resolution lengths are shorter than 0.5°. Apart from the map views, velocities along 4 vertical profiles are shown in Figure 10.

The model slices in Figures 8 and 9 show that in most parts of the Sichuan-Yunnan region under study, the lower crust and the layer immediately below the Moho interface are characterized by relatively low-velocity zones, while the uppermost mantle below 55-km depth generally has average velocity. The overall low-velocity feature can be also seen in the apparent velocities of the Pg and Pn waves based on the linear regression of the traveltime measurements (Figure 5). The average apparent velocity of 4.96 km/s for the Pg arrivals is much

smaller than the global average value of 6.7 km/s in model AK135 (Kennett et al., 1993). The average apparent velocity of 8.07 km/s for the Pn arrivals, which was also reported by other studies (e.g. Pei et al., 2007), is also relatively low as compared with the other regions.

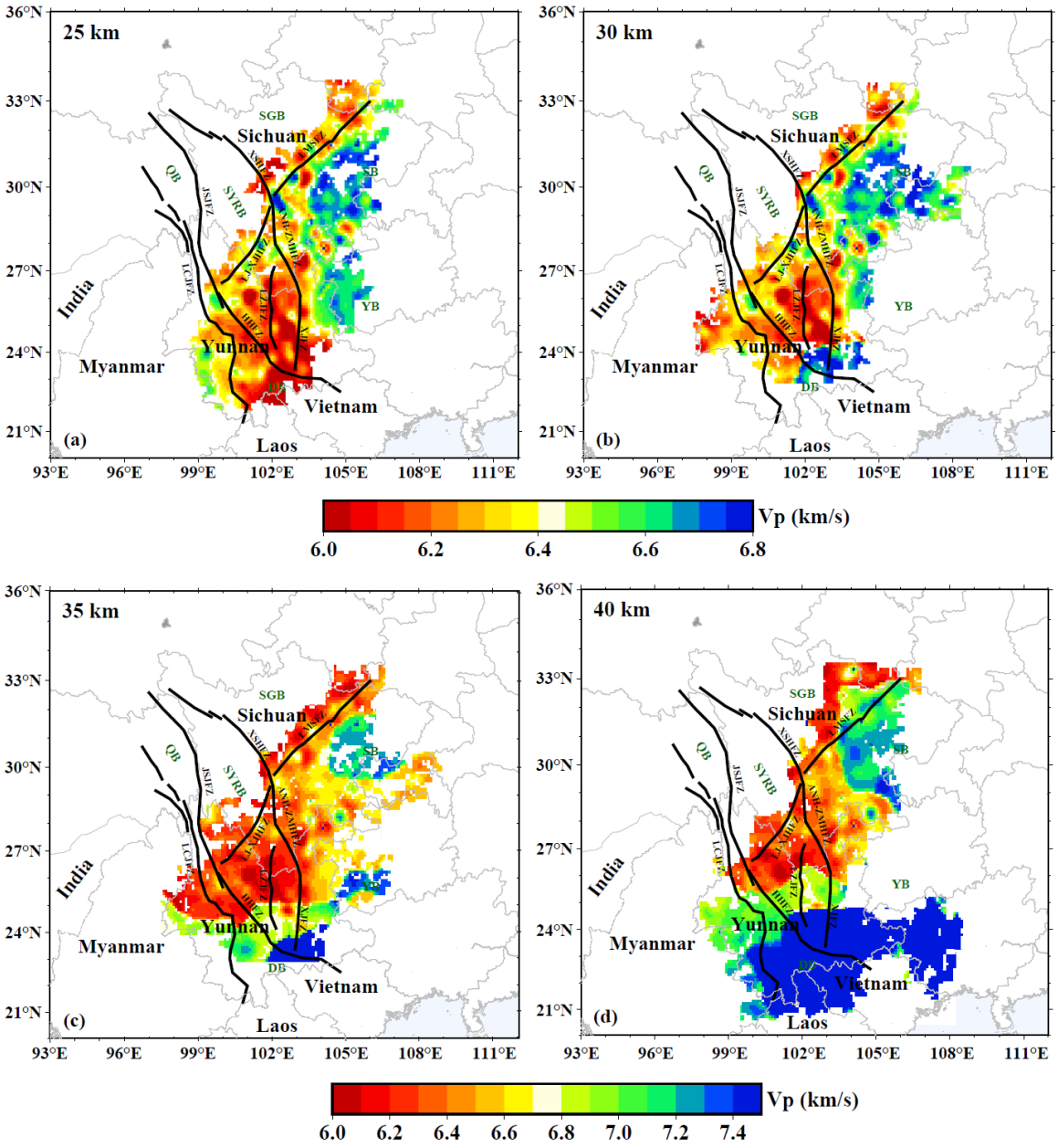

Figure 8 Map of P-wave velocities in our tomography result at depths of (a)

25 km, (b) 30 km, (c) 35 km, and (d) 40 km. Map features are the same as in Figure 4. Note the different color bar ranges for (a-b) and (c-d).

There are regions in the lower crust with rather low P-wave velocities, even below 6.0 km/s, such as the area around 26°N in the Sichuan-Yunnan Rhombic Block; while high velocities can be found in the Sichuan Basin with patches of velocities above 7.2 km/s (Figure 8). In the uppermost mantle, the low-velocity zones with values lower than 7.5 km/s can be found above depth of 55 km and the southeast margin of the low-velocity zone has extremely high velocities above 8.3 km/s (Figure 9).

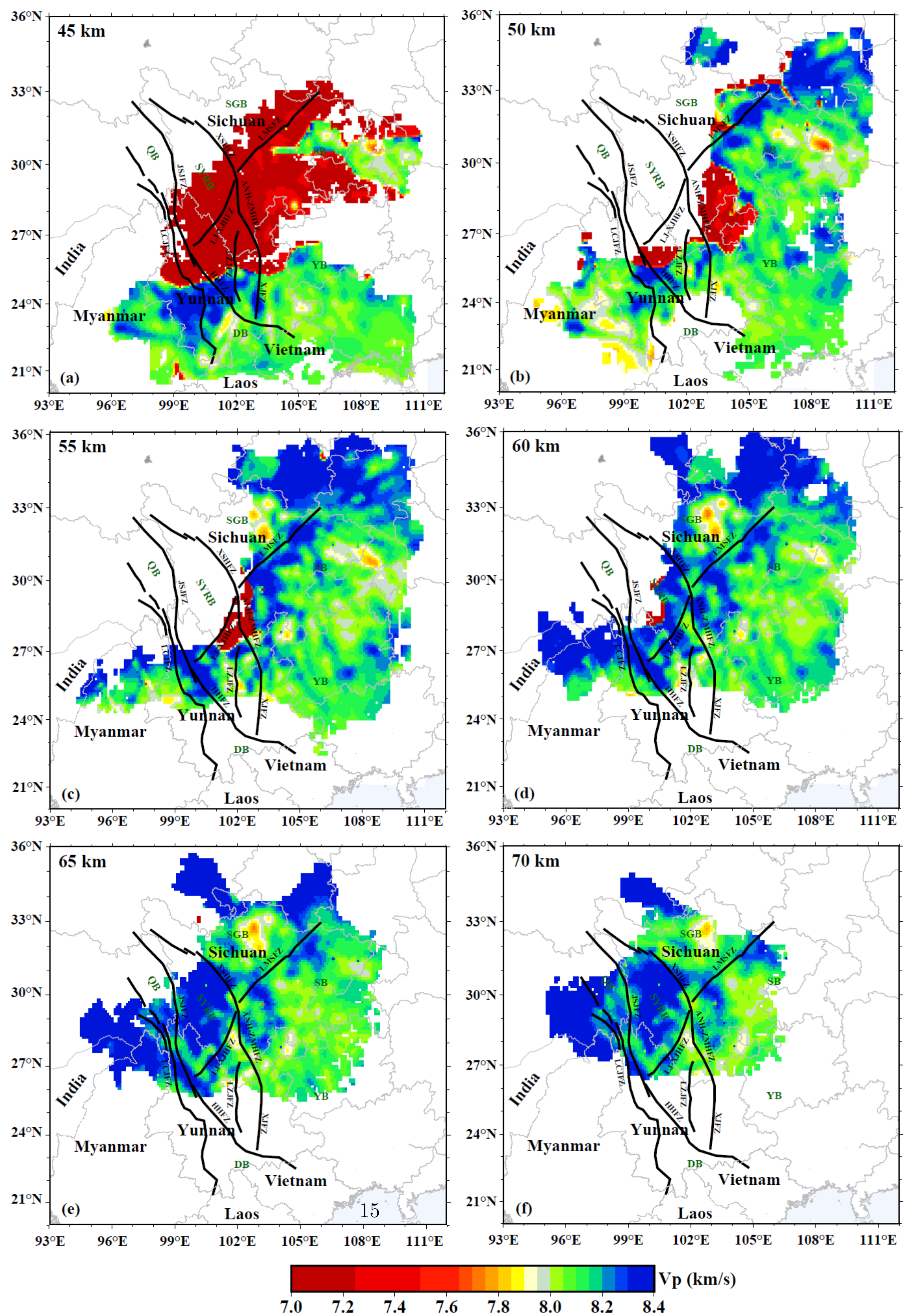
45 km
(a)
50 km
(b)
55 km
(c)
60 km
(d)
65 km
(e)
70 km
(f)
Sichuan
Yunnan
Myanmar
Vietnam
Laos
India
SGB
SB
YB
DB
QB
SYRB
XSHFZ
LMSFZ
ANHFZ
ZMHFZ
LZJFZ
XJFZ
LCJFZ
JSJFZ
HHFZ
36°N
33°N
30°N
27°N
24°N
21°N
93°E
96°E
99°E
102°E
105°E
108°E
111°E
Vp (km/s)
7.0
7.2
7.4
7.6
7.8
8.0
8.2
8.4

Figure 9 Map of P-wave velocities in our tomography result at depths of (a) 45 km, (b) 50 km, (c) 55 km, (d) 60 km, (e) 65 km, and (f) 70 km. Map features are the same as in Figure 4. Note the change in the color bar range from Figure 8.

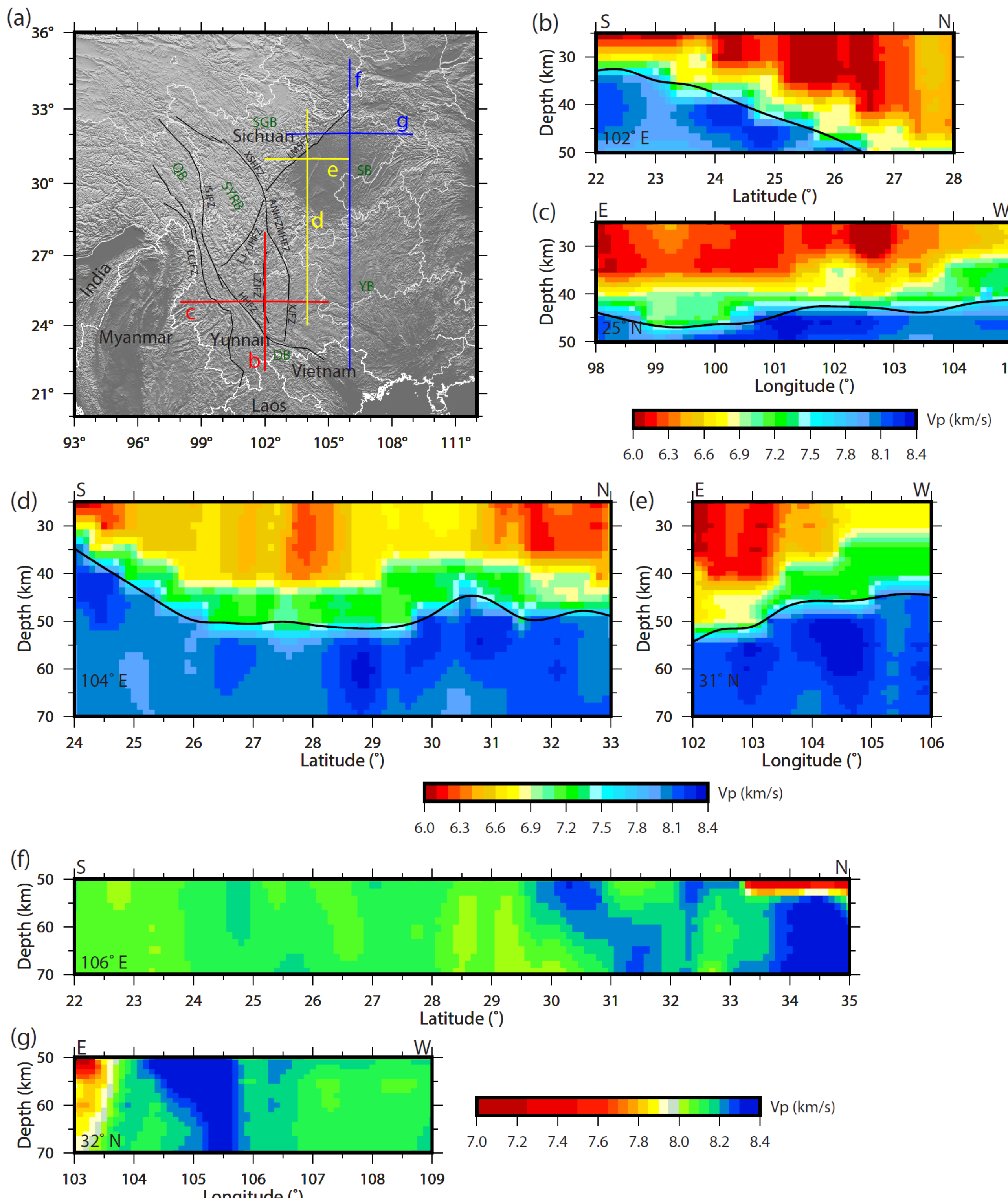

(a)
Sichuan
Yunnan
Myanmar
Vietnam
Laos
India
SGB
SB
YB
QB
SYPB
DB
36°
33°
30°
27°
24°
21°
93°
96°
99°
102°
105°
108°
111°
(b)
102° E
Depth (km)
Latitude (°)
(c)
25° N
Longitude (°)
Vp (km/s)
6.0 6.3 6.6 6.9 7.2 7.5 7.8 8.1 8.4
(d)
104° E
Depth (km)
Latitude (°)
(e)
31° N
Longitude (°)
Vp (km/s)
6.0 6.3 6.6 6.9 7.2 7.5 7.8 8.1 8.4
(f)
106° E
Depth (km)
Latitude (°)
(g)
32° N
Depth (km)
Longitude (°)
Vp (km/s)
7.0 7.2 7.4 7.6 7.8 8.0 8.2 8.4

Figure 10 Vertical profiles of the P-wave velocities in our tomography result. (a) Blue dashed lines labeled b-g show the locations of profiles in (b-g). Map features are the same as in Figure 4. (b-g) P-wave velocity profiles. Black lines denote the Moho interface in LITHO1.0 (Pasyanos et al., 2014). Note the different color bar for profiles (f) and (g).

In contrast to the smooth patterns in the initial model LITHO1.0 in the lower crust and uppermost mantle, strong small-scale anomalies can be seen in our final 3-D P-wave velocity model. Although the depth variation of P-wave speed in the lower crust and uppermost mantle may be complex, regional variation seems consistent at different depths. For instances, the stable Sichuan Basin always exhibits a smooth high-velocity pattern in both the lower crust and uppermost mantle, except for a slightly low-velocity zone between the depths of 50 km and 60 km (Figure 9). The eastern part of the Songpan-Ganzi Block shows low-velocity extending from 55-km to 65-km depth; high-velocity areas across the Longmenshan Fault Zone along 32°N can be seen in the depth range of 50-65 km with a slight shift to the southeast of the fault.

4. Discussion

As can be expected from the many major active zones criss-crossing the region and forming the boundaries between the tectonic blocks, our P-wave velocity model exhibits a highly heterogeneous pattern in the lower crust throughout the Sichuan-Yunnan region. For instance, strikingly different velocities can be seen in the regions located on opposite sides of the Longmenshan Fault Zone and the Anninghe-Zemuhe Fault Zone (ANH-ZMHFZ), with the velocity changing from 6.3 km/s on the western side to above 6.6 km/s on the eastern side over a short distance. Similarly, strong lateral heterogeneities are also present in the uppermost mantle.

Apart from the high velocities in the area around the Sichuan Basin and the Yangtze Block, the lower crust of the Sichuan-Yunnan region is generally characterized by a low-velocity anomaly with a mean value of 6.7 km/s, which is rather low as compared with many other regions in the world. For example, Deng et al. (2014) reported the P-wave speed value of above 7.0 km/s in the lower crust of southeast China, Chulick et al. (2013) yielded a P-wave speed of 6.9-7.3 km/s in the lower crust of South America, and Tesauro et al. (2014) found that the P-wave speed in the lower crust of the North America Continent is generally above 6.8 km/s. As can be seen in Figures 8-10, the P-wave velocity in the top of the uppermost mantle is also much lower than the global average value of 8.04 km/s in model AK135 (Kennett et al., 1993). In the deeper part, the whole region is largely featured by velocities of ~8.1 km/s. This is comparable to many other places, such as the values of 8.15 km/s in northern Eurasia (Schueller et al., 1997) and 8.2 km/s in southeast China (Sun and Kennett, 2016) and South America (Chulick et al., 2013).

As shown in Figure 9, our P-wave tomography model shows a high level of lateral variation in the uppermost mantle (45–50 km) in the southwest region

where the velocity jumps from below 7.5 km/s to above 8.2 km/s over a short distance. In contrast, the Sichuan Basin and the Yangtze Block have weak lateral heterogeneity and are dominated by velocities around 8.1 km/s. The variations of P-wave speed in the uppermost mantle appears to have no apparent relationship with the surface feature, such as the Sichuan Basin. Meanwhile, we cannot see any distinct features in the velocity model marking the major fault zones. This means that those giant faults may not have extended all the way to the Moho. We can also see this in the high velocity band along the Longmenshan Fault Zone which slowly vanishes with increasing depth.

In contrast to the upper mantle, the variation of the complex 3-D P-wave velocity structures in the lower crust is closely related to the regional tectonics. As shown in Figure 8, the old stable Sichuan Basin located to the east of the Longmenshan Fault Zone is characterized by relatively high P-wave velocity at lower crustal depths as compared to other places in the Sichuan-Yunnan region. The Sichuan Basin was an intra-cratonic basin from the late Proterozoic to the middle Late Triassic times (Jia et al., 2006). It has undergone many different phases of changes during its long evolution history, but has always maintained as a single stable block with few large active faults and relatively low seismic activity. In Figure 8, we can see the high-speed feature associated with the stable basin extending from the depth of 25 km to almost 45 km. The stable Sichuan Basin has clearly resisted the eastward movement of the Songpan-Ganzi Block at the Longmenshan Fault Zone. The push between the Tibetan Plateau in the west and the Sichuan Basin in the east results in the drastic relief across the Longmenshan Fault Zone.

Similar to the Sichuan Basin, the Yangtze Block further south is also characterized by higher P-wave speeds in the lower crust. The P-wave velocity in this stable region varies smoothly at different depths (Figure 10f). Because of the resistance of the Sichuan Basin and Yangtze Block, the eastward movement of the Tibetan Plateau is redirected to southward and drives the Sichuan-Yunnan Rhombic Block to rotate clockwise, which can be seen in the velocity field of the crustal deformation observed by GPS in the Sichuan-Yunnan region (Figure 1). The Yangtze Block is not as stable as the older Sichuan Basin, and the resistance may not be as strong as in the Longmenshan Fault Zone, resulting in a much less sharp contrast in topography relief.

To the west of the Longmenshan Fault Zone, the Songpan-Ganzi Block covered by a thick sequence of deep marine deposits is considered to be part of the old Yangtze Platform and underlain by continental crust (e.g., Burchfiel et a1., 1995; Zhang, 2001; Liu et al., 2006). The average P-wave velocity in the eastern margin of this block at lower crustal depths is about 6.2 km/s, with some extremely low-velocity anomalies below 6.0 km/s. These low-velocity features are consistent with the possible existence of lower crustal flow in this region. The low-velocity materials are distributed around the higher-velocity region near the Longmenshan Fault Zone, which may indicate that the flow is blocked by the stable Sichuan Basin and bifercated to both north and south along the fault

zone. Yang et al. (2020) also found the existence of a significantly low-velocity region and suggested that the thickening and erosion of the crust-mantle transition zone may be due to the mixing and metasomatism caused by the partial melt materials in the mid-lower crust. We can also see a region of rather low velocity in the eastern margin of the Songpan-Ganzi Block between the depths of 50 km and 70 km in Figure 10(f). There is a large block of rather high velocity with values above 8.2 km/s extending from 50-km to 70-km depth south of the low-velocity channel beneath the Sichuan Basin. The rather stable basin obviously plays an important role in preventing the materials from flowing further east. Previous studies also found the low-velocity zone in the uppermost mantle and suggested that it is the result of warm material upwelling from the deep mantle based on tomography and anisotropy studies using local and teleseismic data (e.g., Wang et al., 2003; Wang et al., 2010; Lei et al., 2019). Based on our P-wave tomography model, we suggest that the low-velocity anomaly in the lower crust beneath the Songpan-Ganzi Block is resulted from the lower crustal flow. The low-velocity materials in the uppermost mantle of this block may come from the upwelling of warm materials from the deep mantle (Figure 11).

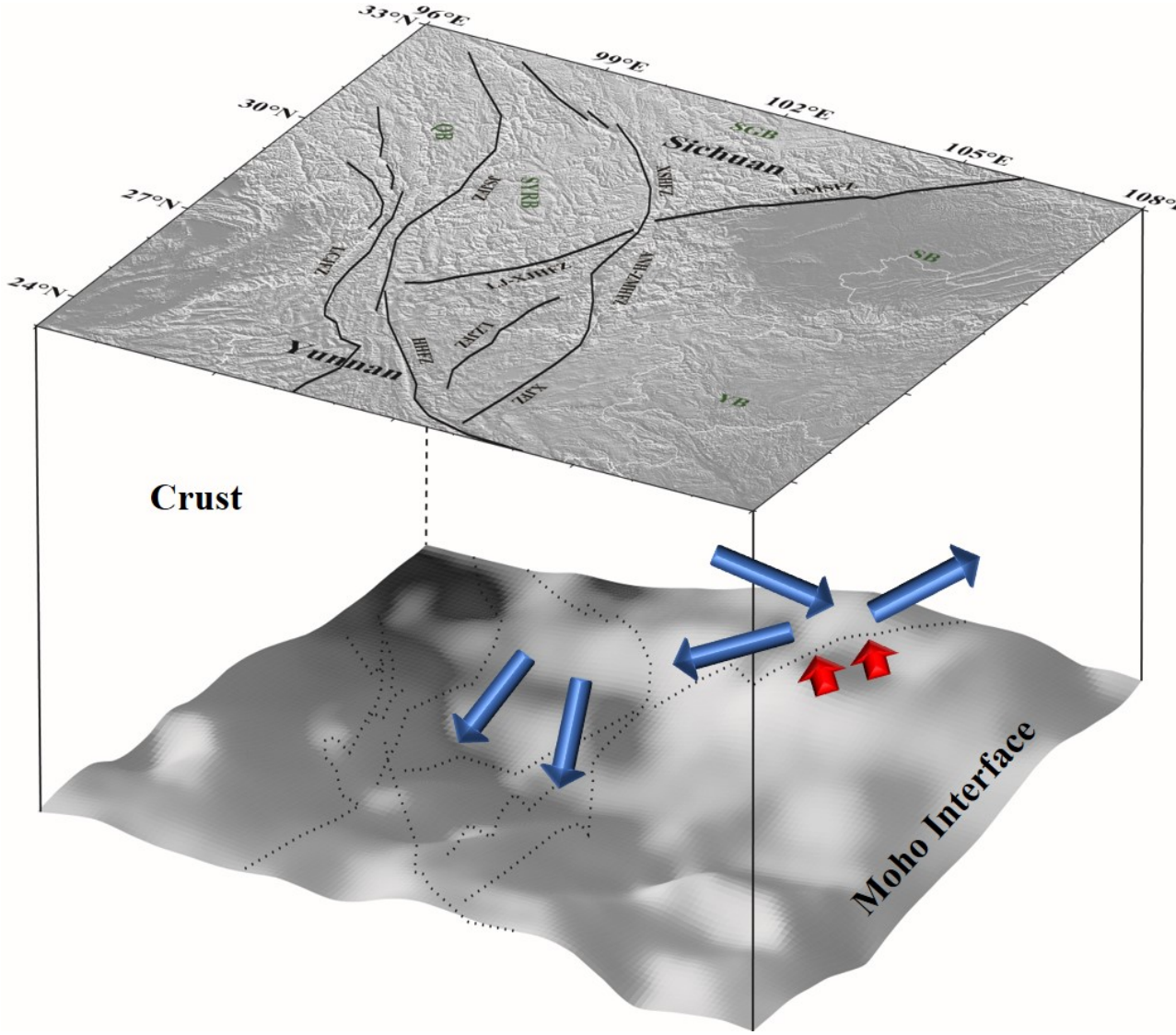

Figure 11 Schematic illustration of the possible material flow beneath the Sichuan-Yunnan region inferred from our tomography model. Blue arrows depict different directions of the lower crustal flow, whereas the red arrows indicate possible upwelling of warm material from the upper mantle beneath the eastern margin of the Songpan-Ganzi Block. The solid and dotted black lines depict the traces of the same major fault zones (as defined in Figure 1) on the surface and Moho, respectively.

In central Sichuan-Yunnan Rhombic Block, there is a low-velocity zone with some extremely slow velocity anomalies (below 6.0 km/s) surrounding the

Lijiang-Xiaojinhe Fault Zone. The rather low-velocity materials may also be indicative of crustal flow in this region. As the upper crust in this region is mainly controlled by brittle deformation (e.g., Wu et al., 2006; Zhang, 2013), the ductile flow of the lower crust may be able to drag the upper crust to move. As a coherent tectonic unit, the Sichuan-Yunnan Rhombic Block is considered to not only have the south-southeast motion, but also a clockwise rotation (e.g., King et al., 1997; Shen et al., 2005). Despite the stress coming from the collision between the Indian and Eurasian plates, the ductile materials in the lower crust also help to drive the whole block to move and rotate. Figure 11 presents an illustrative sketch of the possible lower crustal flow based on the velocity patterns in our 3-D tomography model for the lower crust and uppermost mantle. The ductile flow is obstructed by locally strong crust and redirected to south-southeast, with a wide lateral distribution in the lower crust. The surface features and movements of the Sichuan-Yunnan region is generally associated with the distribution of the lower crustal flow of a large quantity of weak and ductile materials. Therefore, we suggest a coupling between the surface deformation and the material flow in the lower crust.

As we can see in Figures 9 and 10, the P-wave velocity at the shallower part of the uppermost mantle is quite different from that of the deeper part. At the depth of 45 km, the velocities are so slow that over half of the region is dominated by velocities of ~7.2 km/s, which is close to those along the southeastern margin of the model in the lower crust. Therefore, the region immediately below the Moho interface may be strongly influenced by the lower crustal flow, as illustrated by the yellow arrows in Figure 11.

The low-velocity materials in the southwestern corner of our model as shown in Figure 9 seem to be blocked by the surrounding high-velocity zone. The extremely high velocity (above 8.3 km/s) in the Sichuan-Yunnan Rhombic Block may indicate that this region becomes relatively cold and stable in the uppermost mantle below 60-km depth, which suggests that the lower crustal flow may not have obvious influence on the deeper part of the uppermost mantle in this region, except at depths above 60 km near the Moho interface.

5. Conclusions

In this study, we have used 43,540 P-wave traveltimes to build a 3-D velocity model for the lower crust and uppermost mantle beneath the Sichuan-Yunnan region. The traveltime dataset involves Pg and Pn onset times picked automatically by the deep machine learning model PickNet and verified by visual inspection. The two-stage iterative tomography inversion with event relocation greatly reduces the travel-time residuals. Statistical resolution matrix analysis shows that our dataset offers overall resolution lengths of 0.4° in the lower crust and 0.2° in the uppermost mantle.

Our 3-D P-wave tomography model exhibits strong lateral variations in both the lower crust and uppermost mantle. Widespread low-velocity features are seen in the lower crust which may indicate the existence of the lower crustal

flow under the eastern margin of the Tibetan Plateau. The stable Sichuan Basin and the Yangtze Block are underlain by high-velocity structures and may act as a dam blocking the crustal flow in the west from moving further east. Patterns of lateral variation in P-wave velocity in the lower crust are closely associated to the distribution of the tectonic blocks on the surface, whereas the velocities in the uppermost mantle seem to have no relationship with the surface features. The thickening and erosion of crust-mantle transition zone beneath the eastern margin of the Songpan-Ganzi Block may be influenced by both the weak materials in the lower crustal flow and the upwelling of warm materials from the deeper mantle. The low-velocity zone extending from the lower crust to the uppermost mantle east and west of the Sichuan-Yunnan Rhombic Block suggests the materials immediately below the Moho interface may be strongly influenced by the lower crustal flow.

Acknowledgements

This work has been supported by the China Postdoctoral Science Foundation (2019M650317) and the National Natural Science Foundation of China (Grants 41904043; U1939202). Waveforms are downloaded from the data management centers of the Incorporated Research Institutions for Seismology (IRIS, http://www.iris.edu) and the China National Seismic Network at Institute of Geophysics, China Earthquake Administration (SEISDMC, doi:10.11998/SeisDmc/SN). Figures are produced by the Generic Mapping Tools of Wessel and Smith (2013). We thank Professor Jian Wang at the Institute of Geology and Geophysics, Chinese Academy of Sciences for help in using PickNet. The authors acknowledge the course 'English Presentation for Geophysical Research of Peking University (Course #01201110) for help in improving the manuscript.

References

An, M. J., 2012. A simple method for determining the spatial resolution of a general inverse problem. *Geophysical Journal International*, **191**(2), 849-864, doi: 10.1111/j.1365-246X.2012.05661.x.

Backus, G. E. & Gilbert, J. F., 1968. The resolving power of gross earth data. *Geophysical Journal of the Royal Astronomical Society*, **16**, 169-205, doi:10.1111/j.1365-246X.1968.tb00216.x.

Bai, D. H., Unsworth, M. J., Meju, M. A., Ma, X. B., Teng, J. W., Kong, X. R., Sun, Y., Sun, J., Wang, L. F., Jiang, C. S., Zhao, C. P., & Liu, M., 2010. Crustal deformation of the eastern Tibetan plateau revealed by magnetotelluric imaging. *Nature Geoscience*, **3**(5), 358-362 doi: 10.1038/ngeo830.

Bao, X. W., Sun, X. X., Xu, M. J., Eaton, D. W., Song, X. D., Wang, L. S., Ding, Z. F., Mi, N., Li, H., Yu, D. Y., Huang, Z. C., Wang, P., 2015. Two crustal low-velocity channels beneath SE Tibet revealed by joint inversion of Rayleigh wave dispersion and receiver functions. *Earth and Planetary Science Letters*, **415**(5), 16-24, doi:10.1016/j.epsl.2015.01.020.

Barmin, M. P., Ritzwoller, M. H. & Levshin, A. L., 2001. A fast and reliable method for the surface wave tomography, Pure and Applied Geophysics, **158**, 1351-1375, doi: 10.1007/PL00001225.

Burchfiel, B. C. Chen, Z. L. Liu, Y. P., & Royden, R. H., 1995 Tectonics of the Longmen Shan and adjacent regions, central China. *International Geology Review* **37**(8) 661-735, doi: 10.1080/00206819509465424.

Chen, H. P., Zhu, L. B., & Su, Y. J., 2016. Low velocity crustal flow and crust-mantle coupling mechanism in Yunnan, SE Tibet, revealed by 3-D S-wave velocity and azimuthal anisotropy. *Tectonophysics*, **685**, 8-20, doi: 10.1016/j.tecto.2016.07.007.

Chen, M., Huang, H., Yao, H., van der Hilst, R. D., & Niu, F., 2014. Low wave speed zones in the crust beneath SE Tibet revealed by ambient noise adjoint tomography, *Geophys. Res. Lett.*, **41**, 334–340, doi:10.1002/2013GL058476.

Chen, S. F., & Wilson, C. J. L., 1996. Emplacement of the LongmenShan Thrust-Nappe Belt along the eastern margin of the Tibetan Plateau, *Journal of Structural Geology*, **18**(4), 413-430, doi:10.1016/0191-8141(95)00096-V.

Chulick, G. S., Detweiler, S., & Mooney W. D., 2013. Seismic structure of the crust and uppermost mantle of South America and surrounding oceanic basins. *Journal of South American Earth Sciences*, **42**, 260-276, doi: 10.1016/j.jsames.2012.06.002.

Clark, M. K., & Royden, L. H., 2000. Topographic ooze: building the eastern margin of Tibet by lower crustal flow. *Geology*, **28**(8), 703-706, doi: 10.1130/0091-7613(2000)28<703:TOBTEM>2.0.CO;2.

de Kool, M., Rawlinson, N., & Sambridge, M., 2006. A practical grid-based method for tracking multiple refraction and reflection phases in three-dimensional heterogeneous media, *Geophysical Journal International*, **167**, 253–270, doi: 10.1111/j.1365-246X.2006.03078.x.

Deng, Y. F., Zhang Z. J., Badal, J., & Fan, W. M., 2013. 3-D density structure under South China constrained by seismic velocity and gravity data. *Tectonophysics*, **627**, 159-170, doi: 10.1016/j.tecto.2013.07.032.

Duan, Y. H., Wang, F. Y., Zhang, X. K., Lin, J. Y., Liu, Z., Liu, B. F., Yang, Z. X., Guo, W. B., & Wei, Y. H., 2016. Three-dimensional crustal velocity structure model of the middle-eastern north China Craton (HBCrust1.0). *Science China Earth Sciences*, **59**(7), 1477-1488, doi: 10.1007/s11430-016-5301-0.

Jia, D., Wei, G., Chen, Z., Li, B., Zeng, Q., & Yang, G., 2006. Longmen Shan fold-thrust belt and its relation to the western Sichuan Basin in central China: New insights from hydrocarbon exploration, *AAPG Bulletin*, **90**(9), 1425-1447, doi:10.1306/03230605076.

King, R. W., Shen, F., Burchfiel, B. C., Royden, L. H., Wang, E., Chen, Z., Liu, Y., Zhang, X. Y., Zhao, J. X., & Li, Y., 1997. Geodetic measurement of crustal

motion in southwest China. *Geology*, **25**, 179-182. doi:10.1130/0091-7613.

Laske, G., Masters., G., Ma, Z. & Pasyanos, M., 2013. Update on CRUST1.0 - A 1-degree global model of earth's crust. *Geophysical Research Abstracts*, **15**, Abstract EGU2013-2658, doi: 0.6092/1970-9870/128.

Legendre, C., Deschamps, F., Zhao, L., Chen, Q. F., 2015. Rayleigh-wave dispersion reveals crust-mantle decoupling beneath eastern Tibet. *Scientific Reports*, **5**, 16644, doi:10.1038/srep16644.

Lei, J., Li, Y., Xie, F., Teng, J., Zhang, G., Sun, C., & Zha, X., 2014. Pn anisotropic tomography and dynamics under eastern Tibetan plateau, *Journal of Geophysical Research: Solid Earth*, **119**, 2174-2198, doi:10.1002/2013JB010847.

Liu, M., Mooney, W. D., Li, S., Okaya, N., & Detweiler, S., 2006. Crustal structure of the northeastern margin of the Tibetan plateau from the Songpan-Ganzi terrane to the Ordos basin. *Tectonophysics*, **420**(1-2), 253-266, doi: 10.1016/j.tecto.2006.01.025.

Liu, Q. Y., van der Hilst, R. D., Li, Y., Yao, H. J., Chen, J. H., Guo, B., Shao, H. Q., Wang, J., Huang, H., & Li, S. C., 2014. Eastward expansion of the Tibetan Plateau by crustal flow and strain partitioning across faults. *Nature Geoscience*, **7**(5), 361-365, doi: 10.1038/ngeo2130.

Lu, Y., Zhang, Z. J., Pei, S. P., Sandvol. E., Xu, T., & Liang, X. F., 2013. 2.5-Dimensional tomography of the uppermost mantle beneath Sichuan-Yunnan and its surrounding region. *Tectonophysics,* **627**, 193-204, doi: 10.1016/j.tecto.2013.03.008.

Kan, R., Hu, H., Zeng, R., Mooney, W. D., & Mcevilly, T. V. 1986. Crustal structure of Yunnan Province, People' s Republic of China, from seismic refraction profiles. *Science*, **234**(4775), 433-437, doi: 10.1126/science.234.4775.433.

Kennett, B. L. N., & Engdahl, E. R., 1991. Traveltimes for global earthquake location and phase identification. *Geophysical Journal International*, **105**(2): 429-465, doi: 10.1111/j.1365-246X.1991.tb06724.x.

Kennett, B. L. N., Engdahl, E. R., & Buland, R., 1995. Constraints on seismic velocities in the Earth from traveltimes. *Geophysical Journal International*, **122**(1), 108-124, doi:10.1111/j.1365-246X.1995.tb03540.x.

Kennett, B. L. N., Sambridge, M. S., & Williamson, P. R., 1988. Subspace methods for large inverse problems with multiple parameter classes. *Geophysical Journal International*, **94**(2), 237-247, doi: 10.1111/j.1365-246X.1988.tb05898.x.

Pasyanos, M. E., Masters, T. G., Laske, G., & Ma, Z., 2014. LITHO1.0: An updated crust and lithospheric model of the Earth, *Journal of Geophysical Research: Solid Earth*, **119** (3), 2153-2173, doi: 10.1002/2013JB010626.

Pei, S. P., Zhao, J. M., Sun, Y. S., Xu, Z. H., Wang, S. Y., Liu, H. B., Rowe, C. A., Toksoz, M. N., & Gao, X., 2007. Upper mantle seismic velocities and anisotropy in china determined through Pn and Sn tomography. *Journal of Geophysical Research: Solid Earth*, **112**(B5), doi: 10.1029/2006JB004409.

Rawlinson, N., Reading, A. M., & Kennett, B. L. N., 2006. Lithospheric structure of Tasmania from a novel form of teleseismic tomography, *J. Geophys. Res.*, **111**, B02301, doi: 10.1029/2005JB003803.

Rawlinson, N., & Sambridge, M., 2004. Multiple reflection and transmission phases in complex layered media using a multistage fast marching method. *Geophysics*, **69**(5), 1338-1350, doi: 10.1190/1.1801950.

Rawlinson, N., & Urvoy, M., 2006. Simultaneous inversion of active and passive source datasets for 3-D seismic structure with application to Tasmania, *Geophysical Research Letter*, **33**(24), doi:10.1029/2006GL028105.

Ritsema, J., van Heijst, H. J., &Woodhouse, J. H., 2004. Global transition zone tomography, *Journal of Geophysical Research*, **109**, B02302, doi:10.1029/2003JB002610.

Ross, Z. E., Meier, M., & Hauksson, E., 2018. P wave arrival picking and first-motion polarity determination with deep learning. *Journal of Geophysical Research: Solid Earth*, **123**(6), 5120-5129. doi:10.1029/2017JB015251.

Royden, L. H., King, R. W., Chen, Z., & Liu, Y., 1997. Surface Deformation and Lower Crustal Flow in Eastern Tibet. *Science*, **276**(5313), 788-790, doi: 10.1126/science.276.5313.788.

Thurber, C. H., 1983. Earthquake locations and three-dimensional crustal structure in the Coyote Lake Area, Central California, *Journal of Geophysical Research*, **88**(B10), 8226–8236, doi:10.1029/JB088iB10p08226.

Sambridge, M. S., & Kennett, B. L. N., 2001. Seismic event location: nonlinear inversion using a neighbourhood algorithm, *Pure and Applied Geophysics*, **158**(12), 241-257, doi: 10.1007/PL00001158.

Schueller, W., Morozov, I. B., & Smithson, S. B., 1997. Crustal and uppermost mantle velocity structure of northern eurasia along the profile quartz. *Bulletin of the Seismological Society of America*, **87**(2), 414-426, doi: 10.1029/96JB03113.

Shen, Z. K., Lu, J., Wang, M., & Burgmann, R., 2005. Contemporary crustal deformation around the southeast borderland of the Tibetan Plateau. *Journal Geophysical Researches: Solid Earth*, **110**, B11409, doi:10.1029/2004JB003421.

Soldati, G. & Boschi, L., 2005.The resolution of whole Earth seismic tomographic models, *Geophysical Journal International*, **161**(1), 143-153, doi:10.1111/j.1365246X.2005.02551.x.

Sun, W. J., & Kennett, B. L. N., 2016. Uppermost mantle P wavespeed structure beneath eastern China and its surroundings. *Tectonophysics*, **683**, 12-26, doi: 10.1016/j.tecto.2016.06.011.

Tesauro, M., Kaban, M. K., Mooney, W. D., & Cloetingh, S., 2014. NACr14: A 3-D model for the crustal structure of the North American Continent. *Tectonophysics*, **631**, 65-86, doi: 10.1016/j.tecto.2014.04.016.

Tian, X. B., Bai, Z. M., Klemperer, S. L., Liang, X. F., Liu, Z., Wang, X., Yang, X. S., Wei, Y. H., & Zhu, G. H., 2021. Crustal-scale wedge tectonics at the narrow boundary between the Tibetan Plateau and Ordos block. *Earth and Planetary Science Letters*, **554**, 116700, doi:10.1016/j.epsl.2020.116700.

Wang, C. Y., Chan, W. W., & Mooney, W. D., 2003. Three-dimensional velocity structure of crust and upper mantle in southwestern china and its tectonic implications. *Journal of Geophysical Research*, **108**(B9), 2442, doi:10.1029/2002JB001973.

Wang, M., Shen, Z.-K., Wang, Y.-Z., Bürgmann, R., Wang, F., Zhang, P.-Z., Liao, H., Zhang, R., Wang, Q., Jiang, Z.-S., Chen, W.-T., Hao, M., Li, Y., Gu, T., Tao, W., Wang, K, & Xue, L. 2021. Postseismic deformation of the 2008 Wenchuan earthquake illuminates lithospheric rheological structure and dynamics of eastern Tibet. *Journal of Geophysical Research: Solid Earth*, **126**, e2021JB022399. https://doi.org/10.1029/2021JB022399.

Wang, C. Y., Zhu, L. P., Lou, H., Huang, B. S., Yao, Z. X., & Luo, X. H., 2010. Crustal thicknesses and Poisson's ratios in the eastern Tibetan Plateau and their tectonic implications. *Journal of Geophysical Research: Solid Earth*,**115**(B11): B11301, doi: 10.1029/2010JB007527.

Wang, J., Xiao, Z., Liu, C., Zhao, D., & Yao, Z., 2019. Deep learning for picking seismic arrival times. *Journal of Geophysical Research: Solid Earth*, **124**, 6612–6624, doi: 10.1029/ 2019JB017536.

Wang, M., & Shen, Z. K., 2020. Present-day crustal deformation of continental China derived from GPS and its tectonic implications. *Journal of Geophysical Research: Solid Earth*, **125**, e2019JB018774. doi: 10.1029/2019JB018774.

Wang, M. M., Hubbard, J., Plesch, A., Shaw, J. H., & Wang, L. N., 2016. Three-dimensional seismic velocity structure in the Sichuan Basin, China. *Journal of Geophysical Research: Solid Earth,* **121**(2), 1007-1022, doi: 10.1002/2015JB012644.

Wang, Q., Zhang, P. Z., Freymueller, J. T., Bilham, R., Larson, K. M., Lai, X. A., You, X. Z., Niu, Z. J., Wu, J. C., Li, Y. X., Liu, J. N., Yang, Z. Q., & Chen, Q. Z., 2001. Present-day crustal deformation in China constrained by Global Positioning System measurements. *Science*, **294**(5542), 574-577, doi: 10.1126/science.1063647.

Wang, Z., Zhao, D., & Wang, J., 2010. Deep structure and seismogenesis of the north-south seismic zone ins outhwest China, *Journal of Geophysical Research: Solid Earth*, **115**, B12334, doi:10.1029/2010JB007797.

Wei, Z., Kennett, B. L. N., & Sun, W. J., 2018. Sn-wave velocity structure of the uppermost mantle beneath the Australian continent. *Geophysical Journal*

International, **213**(3), 2071-2084, doi: 10.1093/gji/ggy109.

Wei, Z., & Zhao, L., 2019. Lg-Q model and its implication on high-frequency ground motion for earthquakes in the

Sichuan-Yunnan region. *Earth and Planetary Physics*, **3**, 526-536, doi: 10.26464/epp2019054.

Wessel, P., Smith, W. H. F., Scharroo, R., Luis, J., & Wobbe, F., 2013. Generic mapping tools: Improved version released. *Eos Transanction American Geophysical Union*, **94**(45), 409-410, doi:10.1002/2013EO450001.

Wu, J. P., Ming, Y. H., Wang, & C. Y., 2006. Regional waveform inversion for crustal and upper mantle velocity structure below Chuandian region. *Chinese Journal of Geophysics (in Chinese)*, **49**(5), 1369-1376, doi: 10.1007/s11442-006-0415-5.

Xu, X. W., Wen, X. Z., Zheng, R. Z., Ma, W. T., Song, F. M., & Yu, G. H., 2003. Pattern of latest tectonic motion and its dynamics for active blocks in Sichuan-Yunnan region, China. *Science in China*, **46**(2), 210-226 doi: 10.1360/03dz0017.

Yao, H., van der Hilst, R. D., & Montagner, J.-P., 2010. Heterogeneity and anisotropy of the lithosphere of SE Tibet from surface wave array tomography, *J. Geophys. Res.*, **115**, B12307, doi:10.1029/2009JB007142.

Zhang, K. J., 2001. Is the Songpan-Ganzi terrane (central China) really underlain by oceanic crust? *Journal of the Geological Society of India*, **57**(3), 223-230.

Zhang, P. Z., Shen, Z., Wang, M., Gan, W., Bürgmann. R., & Molnar, P., Wang, Q., Niu, Z. J., Sun, J. Z., & Wu, J. C., 2004. Continuous deformation of the Tibetan plateau from global positioning system data. *Geology*, **32**(9), 809-812, doi: 10.1130/G20554.1.

Zhang, P. Z., 2013. A review on active tectonics and deep crustal processes of the Western Sichuan region, eastern margin of the Tibetan Plateau. *Tectonophysics*, **584**, 7-22, doi: 10.1016/j.tecto.2012.02.021.

Zhang, X., & Wang, Y. H., 2009. Crustal and upper mantle velocity structure in Yunnan, Southwest China. *Tectonophysics*, **471**(3-4), 171-185: 10.1016/j.tecto.2009.02.009.

Zhao, L. F., Xie, X. B., He, J. K., Tian, X. & Yao, Z. X., 2013. Crustal flow pattern beneath the Tibetan Plateau constrained by regional Lg-wave Q tomography, *Earth Planetary Science Letter*, **383**, 113-122, doi: 10.1016/j.epsl.2013.09.038.

Zhu, W., & Beroza, G. C., 2019. PhaseNet: A deep-neural-network-based seismic arrival time picking method. *Geophysical Journal International*, **216**, 261-273, doi:10.1093/gji/ggy423.